J. Membrane Biol. 80, 59–70 (1984)

The Journal of
Membrane Biology

Partitioning of Paracellular Conductance Along the Ileal Crypt-Villus Axis: A Hypothesis Based on Structural Analysis with Detailed Consideration of Tight Junction Structure-Function Relationships

Manuel A. Marcial, Susan L. Carlson, and James L. Madara
Department of Pathology (Gastrointestinal Pathology), Brigham and Women's Hospital and Harvard Medical School, Boston, Massachusetts 02115

Summary. Current models of intestinal transport suggest cells which absorb ions are located on the villus while secretory cells are located in the crypt and putatively have paracellular pathways which are highly conductive to Na^+. One approach to assess possible variation in small intestinal paracellular conductance along the crypt-villus axis is to morphometrically analyze the structural aspects of crypt and villus tight junctions (TJs) which relate to paracellular resistance. Such detailed analysis of junctional structure in this heterogeneous epithelium would permit one to compare intestinal TJ structure-function relationships with those in a structurally simpler epithelium such as that of toad urinary bladder. This comparison would also be of considerable interest since previous similar comparisons have failed to consider in detail the geometric dissimilarity between these two epithelia. We applied light, electron microscopic, and freeze-fracture morphometric techniques to guinea pig ileal mucosa to quantitatively assess, for both crypts and villi, linear TJ density, relative surface contributions, and TJ strand counts. Mean linear TJ densities were 76.8 m/cm^2 for crypt cells and 21.8 m/cm^2 for villus absorptive cells. Mean TJ strand counts were 4.45 for undifferentiated crypt cell TJs and 6.03 for villus absorptive cell TJs. The villus constituted 87% and the crypt 13% of total surface. We utilized these data to predict paracellular conductance of crypts *vs.* villi based on equations derived from those of Claude (P. Claude, *J. Membrane Biol.* **39**:219–232, 1978). Such analysis predicts that 73% of ileal paracellular conductance is attributable to the crypt. Furthermore, we obtained literature values for paracellular resistance in mammalian ileum and toad urinary bladder and for toad bladder TJ structure and linear density and constructed a relationship which would allow us to more accurately compare TJ structure-function correlates between these two epithelia. Such a comparison, which considers both surface amplification and TJ structure and distribution in these epithelia, shows that one would predict *in vitro* measured values for paracellular resistance should be approximately two orders of magnitude less in mammalian ileum than in toad urinary bladder. This predicted discrepancy (115-fold) correlates well with the observed difference (100-fold). These findings suggest that highly similar TJ structure-function relationships apply to these geometrically dissimilar tissues and that, in mammalian ileum, the crypt compartment may be responsible for the majority of net ileal paracellular conductance. We speculate that high crypt linear TJ density and low crypt TJ strand counts may serve as the structural basis of massive paracellular Na^+ movement which is coupled to active Cl^- secretion and appears to originate from the crypt following exposure to intestinal secretagogues.

Key Words intestine · tight junction · paracellular pathway · transepithelial resistance

Introduction

A variety of evidence suggests that the continuous intercellular tight junctions, present in non-keratinizing epithelia, are the rate-limiting barrier which restrict free diffusion of ions and water through the paracellular channel (for reviews *see* [24, 25]). Moreover, specific structural aspects of native unperturbed tight junctions such as strand count and depth, as assessed by freeze fracture, generally correlate with the ability of epithelia to resist transepithelial ion flow [4, 28]. However, mammalian small intestine is a widely referenced apparent exception to this general rule. While paracellular resistance of ileal epithelium is two orders of magnitude below that of toad urinary bladder, both epithelia have, on average, somewhat similar tight junction structure [22]. The potential weakness of a comparison such as this is its failure to consider many additional structural features such as serosal-to-mucosal surface amplification, density of junctional pathways per unit surface area, and the degree of heterogeneity of cell structure. All of these variables might potentially exert a major effect on measured paracellular resistance in a heterogeneous, geometrically complex epithelium like that of mammalian ileum. For example, we have previously shown that the absorptive epithelial cells lining the villi of mammalian small intestine display tight junctions which differ structurally from those of secretory undifferentiated crypt cells [21]. Moreover, unlike the flat epithelium of toad bladder, that of mammalian ileum displays a substantial serosal-to-mucosal surface area amplification which would be present in the *in vitro* conditions under which estimates of tissue paracellular conductance are ob-

tained. Indeed, when such additional variables were roughly estimated and considered for a variety of epithelia, there appeared to be an excellent correlation between tight junction structure and passive paracellular flow [3]. Specifically, an arithmetic increase in tight junction strand count appeared to result in a logarithmic increase in paracellular resistance [3]. If this structure-function correlation is correct, one should be able to account for the discrepancy in measured paracellular conductance which exists between the epithelial linings of toad bladder and mammalian ileum by more detailed consideration of the complexity of ileal epithelial structure. Moreover, by applying quantitative structural studies separately to the crypt and the villus, one should be able to estimate the fractional contribution of each epithelial subcompartment to net tissue paracellular resistance and conductance. This would be of considerable interest in the small intestine since the crypt is thought to be the compartment responsible for electrogenic Cl^- secretion and current models for such secretion envision highly conductive paracellular pathways adjacent to the secretory cells [10, 12].

To accomplish the above goals, we applied morphometric techniques to guinea pig ileal epithelium to quantitate all known structural parameters which relate to passive paracellular ion flow. Furthermore, we use these data in equations derived from those of Claude [3] to estimate the relative contributions of crypts and villi to net paracellular conductance in this epithelium. In light of our findings, we discuss the effect that such detailed consideration of paracellular pathway structure would have on structure-function comparisons between geometrically different epithelia. Specifically, we quantitatively reconsider the comparison between toad urinary bladder and mammalian ileal junctional structure and function as a test of the proposed junctional strand count/junctional resistance relationship.

Materials and Methods

General

Fourteen Hartley strain guinea pigs weighing 400 to 600 grams were anesthetized by injecting 5 ml of a saturated urethane solution into the peritoneum. Samples of ileal mucosa, taken 5 to 10 cm from the ileocecal valve, were rapidly fixed for light and electron microscopy by submerging them in a 4°C solution containing 2% formaldehyde, 2.5% glutaraldehyde, and 0.075% $CaCl_2$ in a 0.1 M Na cacodylate buffer at pH 7.4 for 2 hr [16]. Tissues were subsequently postfixed for 1 hr in 1% osmium tetroxide, dehydrated in graded concentrations of alcohols and embedded, without efforts to orient, in Epon. Randomly oriented 1-μm sections were obtained in order to quantitate parameters of surface area as outlined below and nonmucosal tissue was then trimmed from the block. The Epon blocks were subsequently randomly trimmed without knowledge of mucosal orientation and silver thin sections cut with a diamond knife. Sections were mounted on 200 hexagonal mesh copper grids and stained with uranyl acetate and lead citrate.

Adjacent ileal tissue samples were prepared for freeze fracture. This tissue was fixed for one hour in the above fixative at 4°C, washed 3 times in 0.1 M Na cacodylate buffer, embedded in 5% agar and chopped into 150-μm slices with a Smith-Farquhar tissue chopper (Sorvall, Newton, Conn.). After equilibrating for one hour in a solution of 25% glycerol in 0.1 M Na cacodylate buffer, each tissue slice was mounted between two gold disks, rapidly frozen in the liquid phase of partially solidified Freon 22 (N.W. Day Supply, Cambridge, Mass.) and stored in liquid nitrogen. Specimens were fractured at a stage temperature of −110°C under a vacuum of at least 6×10^{-7} mm Hg in a Balzers 300 Freeze-etch device (Balzers, Hudson, N.H.) equipped with a double replica attachment. The fractured tissue was replicated from an angle of 45° with platinum without etching, coated from 90° with carbon, cleaned in commercial bleach and mounted on Formvar-coated (Ernest F. Fullam Co., Schenectady, N.Y.) 200 hexagonal mesh copper grids. Both freeze-fracture replicas and silver thin sections were examined and photographed in a Philips 201 electron microscope (Philips Electronic Instruments, Inc., Mahwak, N.J.) at 60 kV.

Additional ileal tissue samples were fixed for scanning electron microscopy by submerging them in a room temperature solution of 2.5% glutaraldehyde and 0.075% $CaCl_2$ in 0.1 M Na cacodylate buffer at pH 7.4 for 48 hr. Tissues were vigorously rinsed three times in 0.1 M Na cacodylate buffer to remove the adherent surface mucous, post-fixed in 1% osmium tetroxide for 1½ hr under constant agitation and dehydrated in graded alcohols. To view crypt lumenal surfaces, some tissue samples were frozen in liquid nitrogen after post-fixation, fractured with a razor blade at liquid nitrogen temperature and warmed to room temperature before dehydration. Tissues were then critical point dried with carbon dioxide in a Samdri PVT-3 critical point dryer (Tousimis Research Corp., Rockville, Md.), mounted on aluminum stubs, and coated with gold palladium in a Hummer-V vaporizer (Technics, Alexandria, Va.). These tissue samples were examined and photographed in an Amray 1000A scanning electron microscope (Amray Inc., Bedford, Mass.) at 20 kV.

Quantitative Morphometry

Seventeen randomly oriented 1-μm-thick sections of ileum were used to determine the relative surface contributions of villi and crypts to total lumenal surface. Each entire section was photographed with a Zeiss photomicroscope (Carl Zeiss, New York, N.Y.) and photomicrographs were printed at a final magnification of 450×. Morphometric analysis of lumenal surface contributions of crypts and villi relative to total lumenal surface was performed by two different methods, utilizing a Zeiss Videoplan Morphometry Unit (Carl Zeiss, New York, N.Y.) The first method, which examined surface length, consisted of tracing the total surface length for both crypt and villus compartments with the magnetic stylus of the morphometry unit. From the data stored we were then able to calculate percentage contributions to total surface length for both villi and crypts. The second method, measuring surface density, consisted of a stereological point

counting analysis in which we recorded the intercepts of the lumenal surface with the test lines of an overlaid transparent coherent square test lattice [9, 30, 31]. The distance between test points in the lattice was 1.4 cm. From these data we were able to calculate the surface density contribution of villi and crypts to net intestinal surface density [9, 31]. These methods of quantitating lumenal surface by light microscopy do not take into account surface area amplification by microvilli.

We also used the tracing technique to determine the serosal-to-mucosal surface amplification factor in ileal epithelium to facilitate the comparison of paracellular structure-function parameters between ileum and toad bladder (*see* Discussion). To accomplish this, the entire mucosal surface length of a section was measured and then divided by the length of the corresponding, underlying muscularis mucosa. Since our past experience with ileal tissues stripped and mounted in our laboratory [18] or stripped and mounted in other laboratories [5] suggested that serosal-mucosal amplification is reduced by the mounting procedure, we also measured this amplification factor on such mounted tissues. For this, four ileal sheets from four different animals were stripped of their serosa and most of their muscularis propria and mounted in Ussing chambers as previously described [18]. While in the chamber, glutaraldehyde was added both to mucosal and serosal reservoirs to give a final concentration of 2%. After 15 min these tissues, which now kept the shape they had assumed *in vitro,* were removed, fixed for light microscopy as described above, embedded in Epon, and sectioned randomly at 1 μm. These sections were then analyzed as outlined above to determine serosal-mucosal amplification.

Thin sections of silver interference color were used to determine the surface length tight junction density in crypts and villi. Only one section per grid, and one grid per experimental animal were selected for quantitative analysis. The basis for selection was the technical quality of staining and absence of contamination. All lumenal plasma membrane profiles from each section were photographed at a magnification of 7000× and printed at a final magnification of 17,600×. Surface length of villus and crypt compartments was measured by tracing the lumenal surface at the base of the microvilli transecting them. The total number of tight junction images intercepting the lumenal surface of crypts and villi was then recorded. Often the lateral membranes at the level of the tight junction were obliquely sectioned and the image was counted on the basis of an obvious underlying intercellular space associated with an overlying density produced by the obliquely sectioned plasma membranes at the level of the junction. Data were expressed as the number of tight junctions per unit surface length for each compartment.

Since we were uncertain how these values would correlate with tight junction length per unit surface area (i.e. cm of tight junction/cm^2 of surface area, a unit designated as l_p), we defined this relationship in model systems and in villus epithelium. Using graph paper, we constructed model sheets of either 5 or 10 mm squares. For each "cell" (square) size, the true "junctional" length per unit area was measured directly by tracing "cell" perimeters. We then randomly overlaid the graph paper with a transparency containing a 10-cm diameter circle subdivided by 8 test diameters equally spaced at 45° intervals. The test diameters were considered to be analogous to a perpendicularly cut section of the model cell sheet. Thus the number of intercepts of these test lines with the "junctional" profiles would correspond to cell junction images per unit of lumenal surface length as we measured it in thin sections of small intestine. To see if the relationship between these two parameters of junctional density derived by the above methods was the same as one would find in intestinal epithelium with cells that were not square, we also measured villus l_p directly from scanning electron photomicrographs by tracing absorptive cell perimeters and compared this value to that of villus linear surface junctional density derived from transmission electron microscopy of thin sections. In all instances we found that the ratio of l_p values to linear surface junctional density values was approximately 2 (1.98 for 5 mm squares, 1.96 for 10 mm squares, 2.19 for villus absorptive epithelium). Thus, for example, a linear surface junctional density of 50/mm would be the equivalent of an l_p of 100 mm/mm^2. We therefore have made this correction and expressed linear junctional density data as l_p's in the Results section.

To assess the structure of individual tight junctions in crypt and villus compartments, twelve pairs of complimentary freeze-fracture replicas were examined. The technically best replica of each complimentary pair was utilized to evaluate tight junction structure along the crypt-villus axis. All well-replicated tight junction images of widths equivalent to or greater than the approximately 2 cm focusing field at a screen magnification of 10,000× were photographed at a magnification of 20,000×. The negative image was photographically enlarged to a final print magnification of 54,000×. In each electron micrograph the intercellular tight junction strand counts and depths were measured at the center and one-third the distance from each end of the tight junction image. Measurements were made only in those images where the fracture plane included the apical and basal limit of the tight junction. Disconnected free-ending strand segments (fasciae occludentes) were not counted. These data were stored in the computer for statistical analysis.

Equations used for Estimating Partitioning of Paracellular Conductance between Crypts and Villi

To estimate the respective contribution of crypts and villi to net ileal passive transjunctional ion flow, we utilized the following equations of Claude [3] which relate tight junction resistance to tight junction structure:

$$R_j l_p = R_j l_{p_{\min}} \cdot p^{-n} \tag{1}$$

where R_j = the resistance of the tight junction, l_p = linear junctional density per unit surface area, p = a junctional constant derived by Claude [3] (which represents the slope of the line she obtained by plotting the log of the junctional specific resistance against the junctional strand number for a variety of epithelia) and n = the number of junctional strands. Thus $R_j l_p$ represents the specific resistance of a tight junction corrected for tissue-to-tissue variation in l_p, and $R_j l_{p_{\min}}$ represents the hypothetical basal tight junction resistance value (i.e. a junction with no strands). Claude [3] derived the following equation to define $R_j l_{p_{\min}}$:

$$R_j l_{p_{\min}} = \rho\, L/w \tag{2}$$

where ρ is the resistivity of the bulk solution within the junction, L is the height of the junction, and w is the width of the slit. Thus by rearranging Eqs. (1) and (2):

$$R_j = (\rho L/w \cdot p^{-n})(l_p)^{-1}. \tag{3}$$

Since the passive ion permeability or conductance of the junction

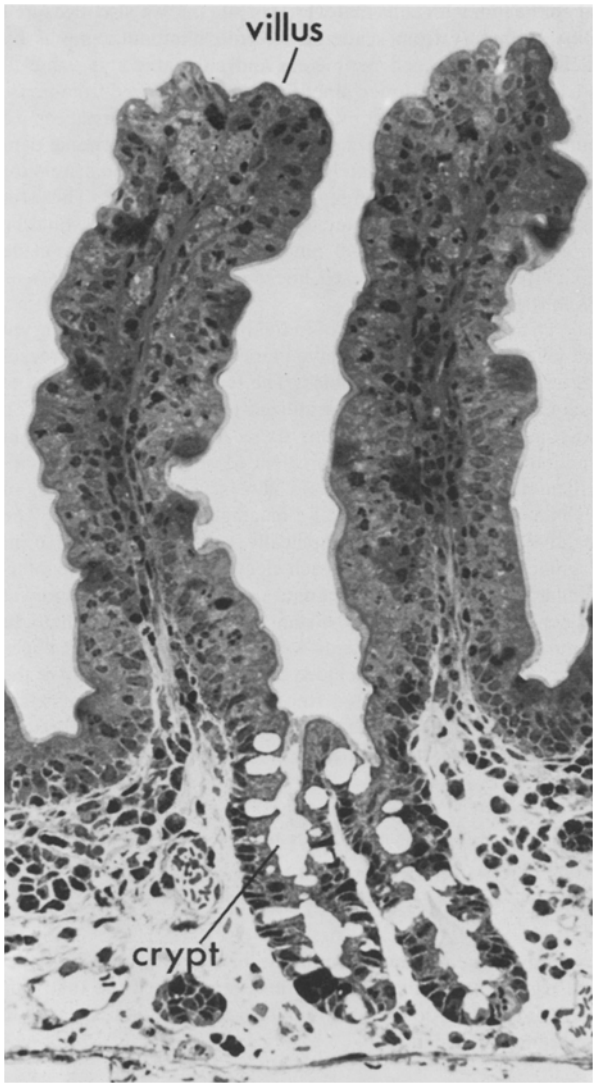

Fig. 1. Light photomicrograph of guinea pig ileal mucosa. A given unit of mucosal length demonstrates a lumenal surface highly enriched in area due to the presence of crypts and villi. However, due to the large surface area of the villus relative to the surface area of the crypt, these two compartments contribute unequally to net intestinal surface (toluidine blue-stained 1-μm section, 275×)

(G_j) would be the reciprocal of R_j, Eq. (3) may be written as

$$G_j = (\rho L/w \cdot p^{-n})^{-1}(l_p). \tag{4}$$

Thus, using the subscripts c and v to represent crypts and villi, respectively, one can express the ratio of crypt-to-villus junctional conductance as

$$\frac{G_{j_c}}{G_{j_v}} = \frac{(\rho L/w \cdot p^{-n})_c^{-1}(l_{p_c})}{(\rho L/w \cdot p^{-n})_v^{-1}(l_{p_v})}. \tag{5}$$

However, surface area is not equally partitioned between crypts and villi. Thus Eq. (5) must be modified by another factor, namely $\frac{S_c/S_t}{S_v/S_t}$ or $\frac{S_c}{S_v}$ where S_c, S_v and S_t refer to the morphometrically determined values for surface densities of the crypts, villi and total surface. If one assumes that the resistivity of the intercellular bulk solution at the level of the tight junction (ρ) is similar for crypts and villi as is the width of the intercellular space at the site of the junction (w), then one can simplify Eq. (5) into the following equation which considers variation from crypts to villi in surface area, tight junction density, tight junction strand count and tight junction depth:

$$\frac{G_{j_c}}{G_{j_v}} = \frac{(L \cdot p^{-n})_c^{-1}}{(L \cdot p^{-n})_v^{-1}} \cdot \frac{(l_{p_c})(S_c)}{(l_{p_v})(S_v)}. \tag{6}$$

Statistical Analysis

Data are expressed in the text as means ± standard error. Statistical significance was evaluated using Students' two tailed t-test.

Results

Light Microscopy

By light microscopy, the mucosa appeared normal and was composed of tall villi lined predominantly by absorptive cells and short crypts lined predominantly by undifferentiated crypt cells (Fig. 1). As seen in Fig. 1, surface area is unequally partitioned between villi (tall wide cylinders) and crypts (short narrow cylinders). Surface length measurements indicated that villi contributed 88% of total surface length and crypts contributed only 12%.

Similarly, stereological point counting analysis indicated that the villus contributed 87% of net intestinal surface density and the crypt 13%. Analysis of serosal-mucosal amplification revealed that the lumenal ileal surface was amplified 7.3× in tissues directly removed from animals and fixed but only 3.25× in tissues mounted and fixed in Ussing chambers. Thus our impression of diminished amplification with mounting was verified. Of interest, although amplification was reduced over 50% by this procedure, crypts and villi were equally affected (11 and 89% surface area contribution for crypts and villi, respectively).

Transmission Electron Microscopy

One hundred ninety electron micrographs of the lumenal surface of crypts and villi were analyzed to assess tight junction densities. Tall columnar villus absorptive cells displaying prominent regular apical microvilli dominated the villus epithelium, and undifferentiated crypt cells with short variable mi-

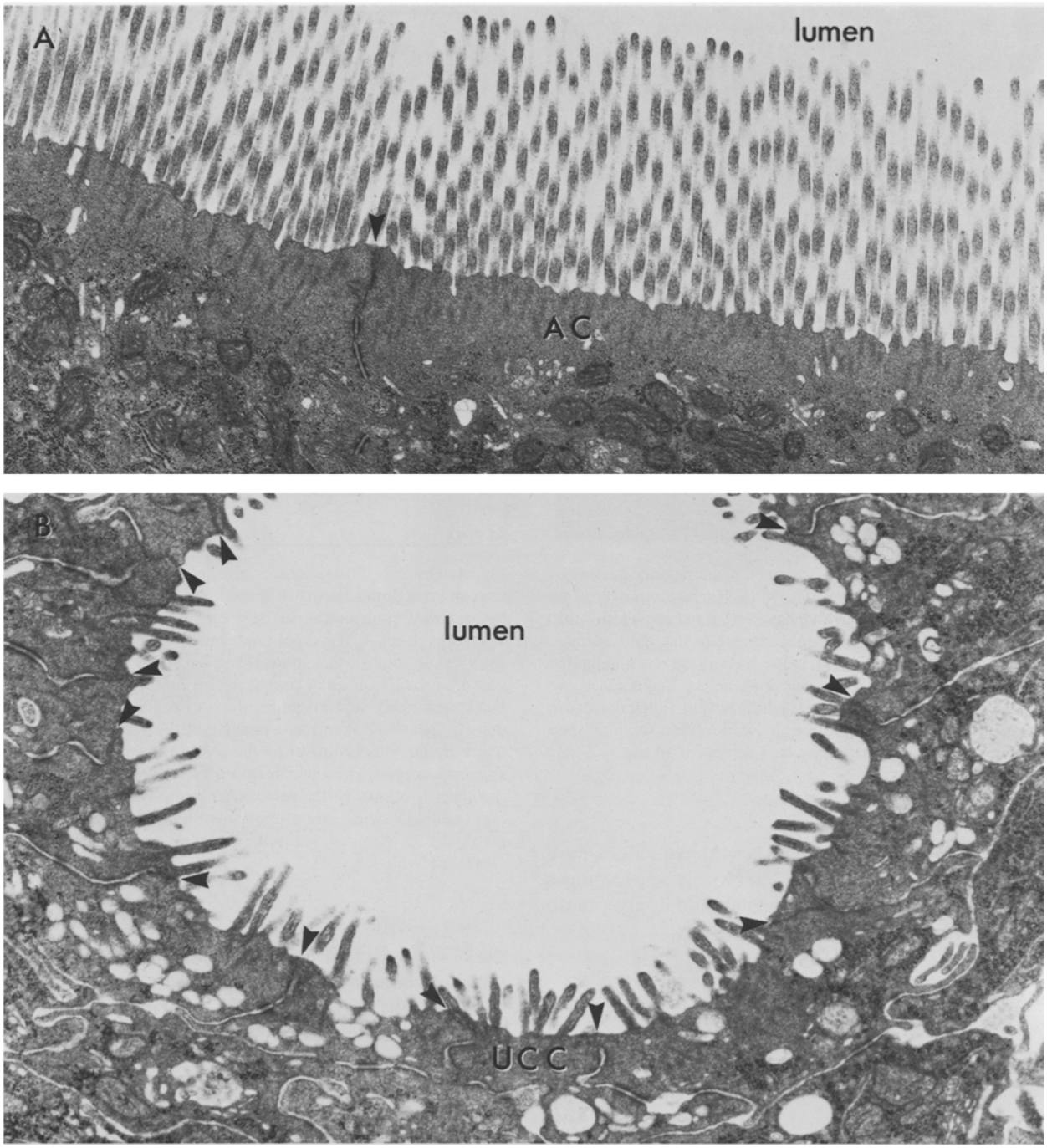

Fig. 2. Transmission electron micrographs of guinea pig ileal villus (*A*) and crypt (*B*) epithelial surface. *A*) Although approximately 10 μm of surface length overlying neighboring villus absorptive cells (*AC*) can be identified, only a single intercellular junctional profile (arrowhead) is seen. *B*) In comparison to the villus, the lumenal surface of crypt epithelium contains numerous intercellular junctional profiles (arrowheads). This photomicrograph of undifferentiated crypt cell (*UCC*) epithelium is of the same magnification as that shown in photomicrograph *A*. (Uranyl acetate, lead citrate, both 17,000×)

crovilli dominated the crypt. A range of zero to three tight junction profiles were seen per electron micrograph of villus epithelium (Fig. 2*A*), while photomicrographs of crypt lumenal borders contained four to sixteen tight junctional profiles (Fig. 2*B*). Quantitative evaluation showed surface length tight junction densities of 109 ± 5.5 tight junctions per mm lumenal surface for villi *versus* 384 ± 27 for

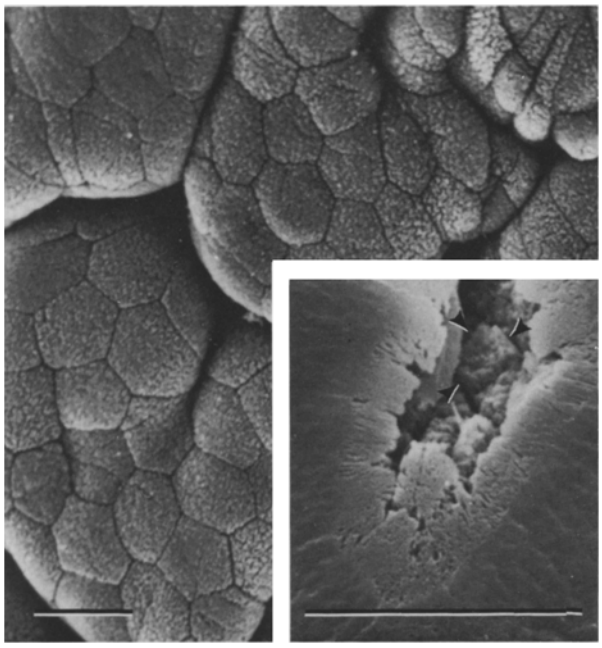

Fig. 3. Scanning electron micrographs of guinea pig ileal villus and crypt (inset) epithelium. The villus surface is covered by polygonal absorptive cells which have estimated cell widths of 10 μm and produce a honeycomb appearance to the villus surface. (1,225×) Inset: Crypt epithelial cells, such as the one highlighted by the arrowheads, are polygonal in shape, but have apical cell widths of only 3.5 μm. Thus the high linear junctional density in the crypt is not due to tortuous cell contours, but to diminished apical cell widths (3,500×). The bars represent 10 μm

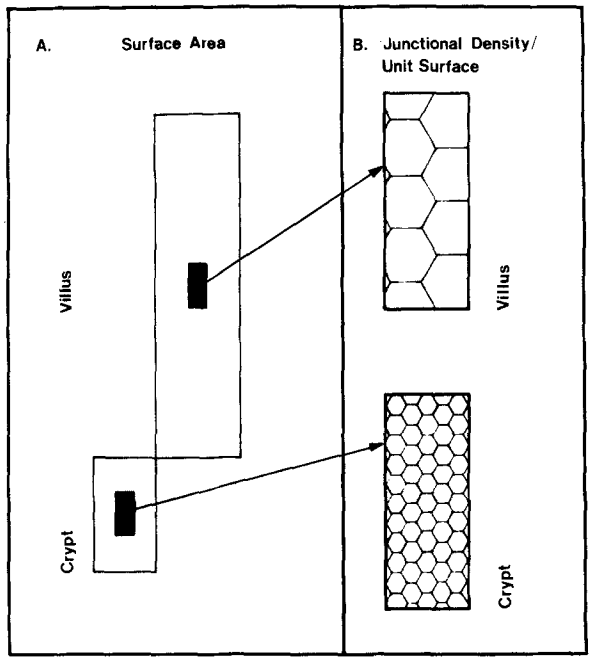

Fig. 4. Graphic illustrations of the interplay between surface area and junctional density in determination of relative paracellular pathway contribution of ileal crypts and villi. As demonstrated in panel *A*, the crypt contributes substantially less than the villus to total surface area. However, if one takes a standard unit of surface from each compartment, represented here by the black rectangles, and magnifies them to examine tight junction density (panel *B*), then one can see that the surface area dominance by the villus is offset by the greater linear junctional density in the crypt. The enrichment of linear junctional density in the crypt is related to the relatively narrow surface diameter of crypt cells. Drawings are proportioned to approximate morphometrically determined variation in these parameters between crypts and villi

crypts ($P < 0.05$). Since we show these values may be multiplied by a factor of 2 to closely approximate l_p, mean l_p's for villi and crypts should approximate 21.8 and 76.8 m/cm^2, respectively.

Scanning Electron Microscopy

A total of 35 scanning electron micrographs, revealing either villus or crypt surfaces were evaluated to determine the geometry of epithelial cell apical borders. Villus absorptive cells were packed in polygonal array and had apical cell diameters of approximately 10 μm (Fig. 3). In contrast, the apical contours of undifferentiated crypt cells were also polygonal, but had approximate apical cell diameters of only 3.5 μm (Fig. 3, inset). In addition, occasional faces of extensively freeze-fractured crypt cell apical membranes showed polygonal crypt cell borders and were thus analogous to the scanning electron microscopic images. Thus the high linear junctional densities seen in the crypt primarily reflected the narrow apex of crypt cells and were not due to striking irregularity of crypt cell apical borders. Thus, the differences in linear junctional density between crypts and villi would offset, in part, the huge surface area fraction contributed by villi in determining the relative net amount of available junctional pathway in each compartment (Fig. 4).

Freeze Fracture

We quantitatively analyzed tight junction depth and strand count in a total of 88 electron micrographs of either villus or crypt junctional images. The villus absorptive cell tight junction was composed of intermeshed, regular strands ranging in number from four to nine (Fig. 5*A*). In contrast, the tight junctions of undifferentiated crypt cells displayed fewer strands, ranging from two to seven (Fig. 5*B*). Many of the crypt cell junctions were irregular and contained loose aberrant strand segments which ended freely on the lateral membrane and were thus not

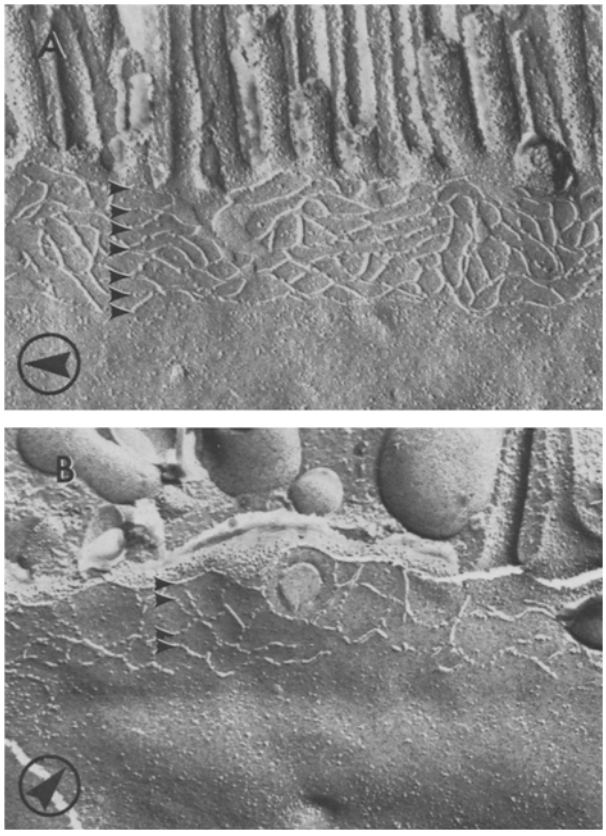

Fig. 5. Electron micrographs of freeze fractured, replicated ileal epithelial tight junctions. *A*) Tight junctions between villus absorptive cells consist of numerous anastomosing P face strands (arrowheads). *B*) In contrast undifferentiated crypt cell tight junctions consist of relatively few such strands (arrowheads) (both 50,000×). The circled arrowheads in the lower left-hand corners indicate the direction of platinum shadowing

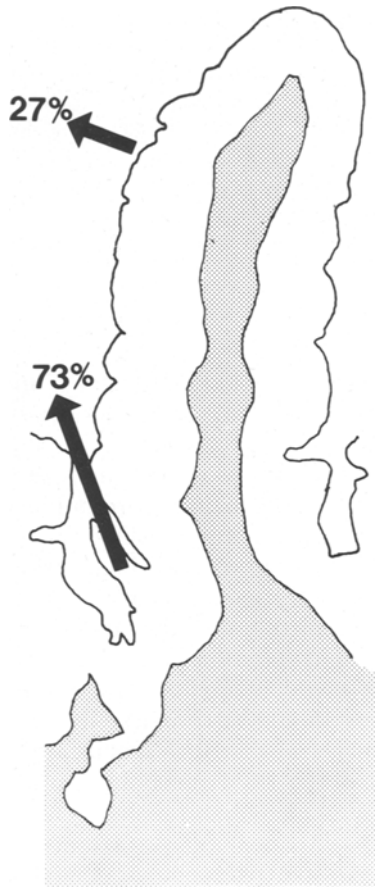

Fig. 6. Diagrammatic illustration of the net impact that junctional pathway structural features should have on the distribution of paracellular conductance along the crypt-villus axis. The major contributor to net paracellular conductance should be the crypt (73%), even though the crypt surface area is small relative to that of the villus

fully incorporated into the tight junction (fascia occludentes). The mean tight junction strand counts were 6.03 ± 0.13 for villus absorptive cells and 4.45 ± 0.16 ($P < 0.05$) for undifferentiated crypt cells. The depth of tight junctions, a parameter which often correlates with strand count, also differed significantly between villus absorptive cells (384 ± 5.8 nm) and undifferentiated crypt cells (236.3 ± 6.7 nm) ($P < 0.05$).

Crypt-Villus Partitioning of Paracellular Ion Conductance

By substituting our experimental values (*see* Table 1) in Eq. (6), we estimated the fraction $\frac{G_{jc}}{G_{jv}}$ to equal 2.72. Solving for percentage contributions of each compartment, we estimate that 73% of net paracellular conductance should take place across the crypt epithelium and only 27% across the villus epithelium (Fig. 6). By omitting consideration of the relative surface area factor in Eq. (6), one may estimate the ratio of crypt-to-villus paracellular conductance per unit of surface area to be 18:1.

Discussion

Although it is possible to morphometrically ascertain precise measurements of various epithelial structural features which relate to paracellular conductance, comprehensive analysis of all such features in an epithelium containing more than a single structurally distinctive compartment and estimation of relative compartmental contributions to net conductance have not previously been performed. Using quantitative morphometric techniques, we de-

Table 1. Morphometrically determined values for structural features of the guinea pig ileal intercellular tight junctions

	Relative surface contribution (%)	Junctions per linear mm of surface, TJ/mm	Junctional length density, *lp* (m/cm^2)	Mean junctional strand count	Mean junctional depth (nm)
Villi	87	109	21.8	6.03 ± 0.13	318.4 ± 5.8
Crypts	13	384	76.8	4.45 ± 0.16	236.3 ± 6.7

fined tight junction structure and density (l_p) in guinea pig ileal crypts and villi. We corrected these data for differences in surface area which exist between crypts and villi. The data were then analyzed in light of basic structure-function correlations which indicate that the degree of paracellular conductance relates (a) positively and arithmetically with the amount of paracellular path available and (b) inversely and logarithmically with the number of strands of individual tight junctions [3]. We thus arrived at a hypothesis which predicts that these two structural domains should have markedly different paracellular ion permeabilities. Specifically, these data suggest that the crypt may display at least an order of magnitude greater paracellullar conductance than the villus per unit surface area. This high degree of passive paracellular conductance in the crypt should more than compensate for the rather limited contribution of the crypt to net surface area, making this compartment the major contributor to ileal paracellular conductance. Since the vast majority of passive ion flow across this epithelium appears to be paracellular [13], these data may also be viewed as suggesting that the majority of ileal transepithelial conductance may be via the crypt. Our estimate of a 73–27% partitioning of paracellular conductance between crypts and villi, respectively, might be modified in a minor way by two other structural considerations. First, we have previously shown that tight junction structure and permeability is heterogeneous among villus goblet cells, and a subpopulation of these cells appear to have tight junctions which are less well formed and more permeable than absorptive cell-absorptive cell tight junctions [20]. We have not considered the presence of such low incidence, potentially high permeability sites on the villus in our calculations since we find guinea pig ileal villus epithelium to have fewer goblet cells (3% by electron microscopic counts of 142 consecutive villus epithelial cells, *unpublished data*) than ileal epithelium of other mammals. However, the more obvious presence of goblet cells in other species would influence our above final calculations albeit in a minor way (12% of rat ileal villus epithelial cells are goblet cells and 23% of villus goblet cell tight junctions have at least one strand count of four or less [20]). Secondly, when the extreme base of small intestinal crypts is revealed in fortunate freeze-fracture planes, one may find tight junctions which have high strand counts, but overall these are of relatively low incidence (*unpublished data*). These sites which might relate to a specific subtype of crypt cell or to an event within the crypt (mitosis) would appear to account for less than 5% of the total crypt junctional pathway. However, even if such sites have markedly low permeabilities, they should not produce more than a 5% overestimate of the net contribution by the crypt to paracellular conductance. Thus, even considering the above caveats, our data would still target the crypts as the major site of paracellular conductance in the ileal epithelium.

Significance of Asymmetric Partitioning of Paracellular Conductance between Crypts and Villi

A variety of evidence indicates that active secretion of ions and water occurs in the intestinal crypt [5, 10, 32]. Additional evidence suggests the following scheme as the likely cellular mechanism of crypt secretion: crypt cells absorb Na^+ and Cl^- across the basolateral membrane, excrete Na^+ into the paracellular space, Cl^- diffusion through the apical membrane maintains electrical equilibrium (an event regulated by secretagogues), and Na^+ moves through the cation-selective tight junction to yield a net serosa-to-mucosa, electrogenic, chloride-dependent secretion of Na^+ and Cl^- [10, 12]. Thus a basic tenet of the above proposal is a paracellular pathway structurally designed to facilitate Na^+ movement from the paracellular space into the lumen. Our data suggests that the crypt might accomplish this feat in two ways—by enriching the surface with available junctional pathway and by producing individual junctions with structural characteristics permitting a high degree of ion permeability.

The above model for secretion of Na^+ and Cl^- has also been applied to secretory epithelia of birds and fishes which live in or must adapt to salt-rich environments. The salt gland principal secretory cells of the salt-stressed domestic duck [29], the chloride-secreting cells of the seawater-adapted killifish operculum [8, 15] and the rectal gland chloride-secreting cells of both the stingray [9] and dogfish shark [9, 11] also show modifications in junctional structure in comparison to adjacent or intermixed nonsecreting epithelial cells. Where these cells interface with each other, they expand the available junctional pathway by assuming markedly irregular interdigitating apical contours. Morphometric analysis reveals that rectal gland secretory epithelium junctional length density (l_p) is 66.9 m/cm^2 in the stingray [9] and ranges from 74.9 to 102 m/cm^2 in the dogfish [9, 11]. Our l_p value for ileal crypt epithelium is 76.8 m/cm^2. Thus, although crypt epithelium expands l_p by a different strategy than that used by the above epithelia (small apical cell diameter rather than irregular contour) the net result is the same. In contrast, l_p in the ileal villus epithelium is 21.8 m/cm^2—a figure closer to that of the "tight," nonsecretory stratified ductal epithelium of the dogfish rectal gland (7.6 m/cm^2) [9]. The individual tight junctions of the above avian and fish secretory epithelia also have few strands although these junctions do differ from those of ileal crypt cells. While crypt cells have irregular junctions with a mean of 4.45 strands, those of avian and fish secretory epithelia have highly characteristic, uniformly structured junctions which consist of two tightly apposed parallel strands.

Since the guinea pig small intestine appears to demonstrate net basal intestinal secretion [26, 27] one might ask how broadly our findings can be applied. Based on our previous experience with rat [17, 20], rabbit [5, 17], monkey [17, 21] and human [19, 21] small intestine we feel these structural features are highly consistent with those found in other mammalian species. We have observed a much greater frequency of tight junction images per unit lumenal length in crypts than on villi in other mammals (*unpublished data*). Moreover, our previous quantitative measurements of ileal absorptive cell and undifferentiated crypt cell tight junction strand counts in monkey ileum [21] are similar to those reported here in guinea pig ileum. Thus a variation in the degree of baseline small intestinal secretion between mammalian species is more likely due to intrinsic difference in undifferentiated crypt cell transport between these species (i.e. higher baseline apical membrane Cl^- permeability, or greater baseline transport rate in guinea pigs) than interspecies variation in the structural features which we describe.

The putative localization of the majority of ileal paracellular conductance in the crypt might also explain, in part, reported osmolality distributions within the lamina propria and would have important implications for *in vitro* transport studies. Cryoscopic techniques used in determining tissue osmolality indicate that during active absorption the lamina propria underlying the villus tips obtains a tissue osmolality of 1,000 to 2,000 mOsm [14]. Moreover, as one approaches the pericrypt lamina propria, this hyperosmolal gradient progressively diminishes [14]. Low villus paracellular conductance would aid in maintaining such local transepithelial ion gradients. Such an interpretation raises the speculative possibility that secondary passive paracellular movements of ions and water may be coupled to active transport at the tissue, but not necessarily at the cellular level within the small intestine. Asymmetric partitioning of paracellular conductance in this epithelium also raises the possibility that *in vitro* short circuiting techniques may not result in a uniform clamping of the transepithelial potential at 0 mV. Rather, a mucosal positive potential would be generated in the crypt while the mucosal negative potential of the villus would not be fully ablated. However, the measured sum of these potentials would be 0 mV. If true, this possibility would tremendously complicate the clear separation of active and passive transport processes in this epithelium.

Comparison of Tight Junction Structure and Function—Small Intestine vs. Urinary Bladder Revisited

Although many data support strongly the validity of estimating paracellular conductance based on structural analysis of tight junctions (for reviews *see* [24, 25]), such associations have been challenged. In a widely quoted paper, Martinez-Palomo and Erlij [22] found that while mammalian small intestinal epithelium and toad urinary bladder epithelium had "similar" tight junction strand counts, they had markedly dissimilar paracellular resistances [22]. Thus, while the ratio (bladder/ileum) of measured paracellular resistances between these two tissues was 100 (12,000/120 Ω cm^2), the ratio of structural parameters of paracellular resistance was only 1.3 (8.7/6.7 strands). However, this study did not consider the heterogeneity of the small intestine with respect to tight junction structure and also did not consider the serosal/mucosal surface amplification which occurs in the small intestine but not in the urinary bladder. A reassessment of the comparison between small intestine and urinary bladder junctional structure and function would be of interest since we

Table 2. Conversion of tight junction strand counts into arbitrary standard units of specific junctional resistance ($R_j l_p$)

	Strand counts	$R_j l_p$[d] $\Omega \cdot$ unit[e]
Toad bladder	8.7[b]	8×10^6
Guinea pig ileum		
Villus	6.03[c]	7.3×10^5
Crypt	4.45[c]	4×10^4 [f]

[a] $R_j l_p$ values are read from the graph prepared by Claude (ref. 3, Fig. 4).
[b] From ref. [22].
[c] From present study.
[d] Specific junctional resistance which correlates to strand counts given; from graph of Fig. 4, ref. [3].
[e] Since data will ultimately be expressed as a ratio, $R_j l_p$ is expressed as an arbitrary unit which is normalized to toad bladder and ileal villus epithelium (*see* text).
[f] The $R_j l_p$ value for the crypt was divided by 3.57 to normalize this value to those of villus and toad bladder [i.e. l_p is similar between these latter two epithelia (ref. 3), but increased 3.57-fold in crypt epithelium (Table 1)].

Table 3. Calculation of predicted discrepancy in paracellular resistance of toad urinary bladder *versus* mammalian ileum and comparison with discrepancy of measured paracellular resistance in these two epithelia[a]

A) Calculation of mean specific junctional resistance ($R_j l_p$) for ileum

$$1/R_j l_{p_i} = (1/R_j l_{p_c})(f_c) + (1/R_j l_{p_v})(f_v) = 0.44 \times 10^5/\Omega \cdot \text{unit}$$

$$R_j l_{p_i} = 2.25 \times 10^5\ \Omega \cdot \text{unit}$$

B) $R_j l_{p_t} = 8 \times 10^6\ \Omega \cdot$ unit

C) Correction of $R_j l_p$'s for surface amplification

$$\frac{R_j l_{p_i}}{S_{\text{amp}i}} = 6.93 \times 10^4\ \Omega \cdot \text{unit}$$

$$\frac{R_j l_{p_t}}{1} = 8 \times 10^6\ \Omega \cdot \text{unit}$$

D) Predicted magnitude of paracellular resistance difference, toad urinary bladder *vs.* mammalian ileum

$$\frac{R_j l_{p_t}}{R_j l_{p_i}} = 115$$

E) Measured magnitude of paracellular resistance difference, toad urinary bladder *vs.* mammalian ileum

$$\frac{R_{p_t}}{R_{p_i}} = 110$$

[a] The ratio of the predicted paracellular resistances derived from structural studies of these epithelia closely approximates the ratio of the measured values for paracellular resistance. For detailed discussion *see* text. Subscripts *c, v, t, i*—refer to crypt, villus, toad bladder, ileum, respectively. f = % surface contribution, from Table 1. $R_j l_p$ values for crypt, villus, and toad bladder from Table 2. S_{amp} = serosal-mucosal surface amplication, *see* text. R_p = measured paracellular resistance values; same as those referenced in comparison in ref. [22].

now have the necessary additional data on the heterogeneous ileal epithelium to make such a comparison meaningful. Such an exercise would also serve as a test of Claude's [3] hypothesis regarding the relationship between junctional strand count and junctional resistance. This comparison, outlined in Tables 2 and 3, was accomplished in the following manner: our tight junction strand counts for villus and crypt cells and Martinez-Palomo and Erlij's [22] strand counts for toad urinary bladder epithelial cells were used to determine the relative predicted junctional resistances (Table 2) as obtained from the graph in Figure 4 of Claude's study [3]. However, Claude's values were corrected for l_p variation from tissue to tissue, and, while cell diameter and estimated l_p's are similar between villus absorptive cells and urinary bladder cells [3], there is a 3.57-fold enrichment of l_p in the crypt. Thus, to normalize the crypt specific junctional resistance to that of villus and toad bladder, one must multiply the former by 0.28. Since the crypt and villus may be viewed as two types of resistors in parallel which are present at two different frequencies (i.e. share intestinal surface nonequally), one may use the crypt and villus junctional specific resistance values to calculate a mean junctional specific resistance for the intestinal epithelium (Table 3). However, while *in vitro* measurements of toad bladder paracellular resistance are representative of a mucosal surface area identical to that of the chamber area used, ileal measurements are not. Thus, we must divide our ileal junctional resistance value by 3.25 to correct for the error expected in the measured paracellular resistance value. The resulting values for ileal and urinary bladder specific junctional resistance can now be expressed as a ratio which, if the structure-function correlations used are accurate, should also represent the ratio of "measured" values of paracellular resistances in these two epithelia. We utilized the same literature values for estimated paracellular resistances as Martinez-Palomo and Erlij [22] in making this comparison. As seen in Table 3, detailed structural analysis *predicts* that ileal epithelium per unit of serosal area should have 115× or approximately 2 logs less paracellular resistance than the same serosal area unit of toad urinary bladder. The actual values indicate that such a unit of ileal epithelium does indeed have 2 logs less paracellular resistance than that of urinary bladder. From this comparison one may conclude that detailed consideration of junctional structure in these epithelia strongly supports, rather than debunks, the correlation between tight junction strand count and tight junction resistance. Furthermore, given the apparent accuracy of this relationship, it is likely

that the precise figures determined in our predicted distribution of paracellular conductance along the crypt-villus axis may have a relatively low degree of inherent error. Rather, the potential sources of error previously outlined may well represent the major source of error in such an analysis.

Other comparisons utilized to probe the structure-function relationships of the intercellular junctional shunt pathway in normal tissues often fail to consider one or more of the above outlined pitfalls or do not really address the issue implicitly suggested. For example, a study which reports a lack of correlation between tight junction structure and permeability properties in developing, compared with adult, sheep choroid plexus [23] has been frequently cited as refuting the notion of a correlation between junctional strand counts and transjunctional resistance to passive ion flow [2, 7, 25]. In fact, these authors report that junctional strand counts are not significantly different at these two time periods while transepithelial flux of macromolecules is widely discrepant [23]. On the basis of available studies of protein movement through fetal choroid plexus epithelium, the authors go on to suggest that such movement is most likely transcellular, perhaps through a fetal transcellular cisternal shunt [23]. Therefore, this widely quoted study does not address directly the issue of transjunctional resistance in the choroid plexus.

We feel that although exceptions to the general relationship between tight junction strand count and transjunctional resistance in unperturbed epithelia may exist, they have, to date, not been convincingly identified. This may not be the case in perturbed epithelia. Martinez-Palomo and Erlij [22] also showed that exposure of toad urinary bladder to mucosal solutions made hypertonic by the addition of either 120 mM lysine or 2 M urea resulted in a decrease in transepithelial resistance [22]. However, while the urea stressed bladders showed extensive perturbation of tight junction structure, the lysine-loaded bladders had morphologically normal tight junctions even though parallel tracer studies utilizing lanthanum were interpreted as indicating that lysine acted solely by increasing paracellular, not transcellular, passive ion diffusion [22]. Although this study indicates a potential difficulty may exist in correlating tight junction structure with function in perturbed epithelia, many other models exist in which such correlations still seem to hold. For example, we have recently shown that the short-term rise in jejunal transepithelial resistance induced by mucosal osmotic loads is paralleled by recruitment of additional junctional elements into absorptive cell tight junctions [18]. Similar alterations in tight junction structure have also been demonstrated accompanying the cyclic AMP-induced resistance increases in gallbladder epithelium [6] and accompanying the resistance increase induced both by plant cytokinins and cytochalasins in this epithelium [1].

This work was supported by research grant AM27972 from the National Institutes of Health and National Research Service Individual Fellowship AM07012. Dr. Madara is supported, in part, by an American Gastroenterological Association/Industry Research Scholar Award. We are grateful to Dr. Jerry S. Trier for critically reviewing this manuscript.

References

1. Bentzel, C.J., Hainau, B., Ho, S., Hui, S.W., Edelman, A., Anagnostopoulos, T., Beneditti, E.L. 1980. Cytoplasmic regulation of tight-junction permeability: Effect of plant cytokinins. *Am. J. Physiol.* **239:**C75–C89
2. Bullivant, S. 1982. Tight junction structure and development. *In:* The Paracellular Pathway. S.E. Bradley and E.F. Purcell, editors. p. 18. Josiah Macy, Jr., Foundation, New York
3. Claude, P. 1978. Morphological factors influencing transepithelial permeability: A model for the resistance of the *zonula occludens*. *J. Membrane Biol.* **39:**219–232
4. Claude, P., Goodenough, D.A. 1973. Fracture faces of zonulae occludentes from "tight" and "leaky" epithelia. *J. Cell Biol.* **58:**390–400
5. Donowitz, M., Madara, J.L. 1982. Effect of extracellular calcium depletion on epithelial structure and function in rabbit ileum: A model for selective crypt or villus epithelial cell damage and suggestion of secretion by villus epithelial cells. *Gastroenterology* **83:**1231–1243
6. Duffey, M.E., Hainau, B., Ho, S., Bentzel, C. J. 1981. Regulation of epithelial tight junction permeability by cyclic AMP. *Nature (London)* **204:**451–453
7. Erlij, D. 1982. Discussion *In:* The Paracellular Pathway. S.E. Bradley and E.F. Purcell, editors. p. 31. Josiah Macy, Jr. Foundation, New York
8. Ernst, S.A., Dodson, W.C., Karnaky, K.J., Jr. 1980. Structural diversity of occluding junctions in the low-resistance chloride secreting opercular epithelium of seawater-adapted killifish (*Fundulus heteroclitus*). *J. Cell Biol.* **87:**488–497
9. Ernst, S.A., Hootman, S.R., Schreiber, J.H., Riddle, C.V. 1981. Freeze-fracture and morphometric analysis of occluding junctions in rectal glands of elasmobranch fish. *J. Membrane Biol.* **58:**101–114
10. Field, M. 1981. Secretion of electrolytes and water by mammalian small intestine. *In:* Physiology of the Gastrointestinal Tract. L.R. Johnson, J. Christensen, M.I. Grossman, E.D. Jacobson and S.G. Schultz, editors. pp. 963–982. Raven, New York
11. Forrest, J.N., Jr., Boyer, J.L., Ardito, T.A., Murdaugh, H.V., Jr., Wade, J.B. 1982. Structure of tight junctions during Cl secretion in the perfused rectal gland of the dogfish shark. *Am. J. Physiol.* **242:**C388–C392
12. Frizzell, R.A., Field, M., Schultz, S.G. 1979. Sodium-coupled chloride transport by epithelial tissues. *Am. J. Physiol.* **236:**F1–F8
13. Frizzell, R.A., Schultz, S.G. 1972. Ionic conductances of

extracellular shunt pathway in rabbit ileum. Influence of shunt on transmural sodium transport and electrical potential differences. *J. Gen. Physiol.* **59:**318–346
14. Jodal, M., Hallback, D-A., Lundgren, O. 1978. Tissue osmolality in intestinal villi during luminal perfusion with isotonic electrolyte solutions. *Acta Physiol. Scand.* **102:**94–107
15. Karnaky, K.J., Jr. 1980. Ion secreting epithelia: Chloride cells in the head region of Fundulus heteroclitus. *Am. J. Physiol.* **238:**R185–R198
16. Karnovsky, M.J. 1965. A formaldehyde-glutaraldehyde fixative of high osmolality for use in electron microscopy. *J. Cell Biol.* **27:**137a
17. Madara, J.L. 1982. Cup cells: Structure and distribution of a unique class of epithelial cells in guinea pig, rabbit, and monkey small intestine. *Gastroenterology* **83:**981–994
18. Madara, J.L. 1983. Increases in guinea pig small intestinal transepithelial resistance induced by osmotic loads are accompanied by rapid alterations in absorptive cell tight junction structure. *J. Cell Biol.* **97:**125–136
19. Madara, J.L., Trier, J.S. 1982. Structural abnormalities of jejunal epithelial cell membranes in celiac sprue. *Lab. Invest.* **43:**254–261
20. Madara, J.L., Trier, J.S. 1982. Structure and permeability of goblet cell tight junctions in rat small intestine. *J. Membrane Biol.* **66:**145–157
21. Madara, J.L., Trier, J.S., Neutra, M.R. 1980. Structural changes in the plasma membrane accompanying differentiation of epithelial cells in human and monkey small intestine. *Gastroenterology* **78:**963–975
22. Martinez-Palomo, A., Erlij, D. 1975. Structure of tight junctions in epithelia with different permeability. *Proc. Natl. Acad. Sci. USA* **72:**4487–4491
23. Mollgard, K., Malinowska, D.H., Saunders, N.R. 1976. Lack of correlation between tight junction morphology and permeability properties in developing choroid plexus. *Nature (London)* **264:**293–294
24. Neutra, M.R., Madara, J.L. 1982. The structural basis of intestinal ion transport. *In:* Fluid and Electrolyte Abnormalities in Exocrine Glands in Cystic Fibrosis. P.M. Quinton, J.R. Martinez and U. Hopfer, editors. pp. 194–226. San Francisco Press, San Francisco
25. Powell, D.W. 1981. Barrier function of epithelia. *Am. J. Physiol.* **241:**G275–G288
26. Powell, D.W., Binder, H.J., Curran, P.F. 1972. Electrolyte secretion by the guinea pig ileum *in vitro*. *Am. J. Physiol.* **223:**531–537
27. Powell, D.W., Malawer, S.J., Plotkin, G.R. 1968. Secretion of electrolytes and water by the guinea pig small intestine *in vivo*. *Am. J. Physiol.* **215:**1226–1233
28. Pricam, C., Humbert, F., Perrelet, A., Orci, L. 1974. A freeze-etch study of the tight junctions of the rat kidney tubules. *Lab. Invest.* **30:**286–291
29. Riddle, C.V., Ernst, S.A. 1979. Structural simplicity of the *zonula occludens* in the electrolyte secreting epithelium of the avian salt gland. *J. Membrane Biol.* **45:**21–35
30. Weibel, E.R. 1979. Stereological Methods—Practical Methods for Biological Morphometry. Academic, London
31. Weibel, E.R., Bolender, R.P. 1973. Stereological techniques for electron microscopic morphometry. *In:* Principles and Techniques for Electron Microscopy: Biological Applications. M.A. Hayat, editor. Vol. 3, p. 237. Van Nostrand Reinhold, New York
32. Welsh, M.J., Smith, P.L., Fromm, M., Frizzell, R.A. 1982. Crypts are the site of intestinal fluid and electrolyte secretion. *Science* **218:**1219–1221

Received 15 September 1983; revised 13 December 1983